Structure-based Analysis of VDAC1 Protein
DEFINING OLIGOMER CONTACT SITES[*]

Shay Geula[‡], Hammad Naveed[§], Jie Liang[§], and Varda Shoshan-Barmatz[‡1]

From the [‡]Department of Life Sciences and the National Institute for Biotechnology in the Negev, Ben-Gurion University of the Negev, Beer-Sheva 84105, Israel and the [§]Department of Bioengineering, University of Illinois, Chicago, Illinois 60607

Background: VDAC1 was shown to undergo oligomeric assembly, an event that is coupled to apoptosis induction.
Results: Structure- and computation-based predications of VDAC1 oligomerization sites were confirmed.
Conclusion: Upon apoptosis induction, VDAC1 undergoes conformational changes and oligomerization.
Significance: Dissection of VDAC1 dimerization/oligomerization provides structural insight into the oligomeric status of cellular VDAC1 under physiological and apoptotic conditions.

The outer mitochondrial membrane protein, the voltage-dependent anion channel (VDAC), is increasingly implicated in the control of apoptosis. Oligomeric assembly of VDAC1 was shown to be coupled to apoptosis induction, with oligomerization increasing substantially upon apoptosis induction and inhibited by apoptosis blockers. In this study, structure- and computation-based selection of the predicated VDAC1 dimerization site, in combination with site-directed mutagenesis, cysteine replacement, and chemical cross-linking, were employed to identify contact sites between VDAC1 molecules in dimers and higher oligomers. The predicted weakly stable β-strands were experimentally found to represent the interfaces between VDAC1 monomers composing the oligomer. Replacing hydrophobic amino acids with charged residues in β-strands 1, 2, and 19 interfered with VDAC1 oligomerization. The proximity of β-strands 1, 2, and 19 within the VDAC1 dimer and the existence of other association sites involving β-strand 16 were confirmed when a cysteine was introduced at defined positions in cysteineless VDAC1 mutants, together with the use of cysteine-specific cross-linker bis(maleimido)ethane. Moreover, the results suggest that VDAC1 also exists as a dimer that upon apoptosis induction undergoes conformational changes and that its oligomerization proceeds through a series of interactions involving two distinct interfaces. Dissection of VDAC1 dimerization/oligomerization as presented here provides structural insight into the oligomeric status of cellular VDAC1 under physiological and apoptotic conditions.

The voltage-dependent anion channel (VDAC)[2] in the outer mitochondrial membrane is a multifunctional channel protein mediating cross-talk between the mitochondria and the cytosol. VDAC1 regulates mitochondrial membrane permeability to ions and small molecules, such as Na^+, K^+, Ca^{2+}, Cl^-, ATP, NADH, succinate, and malate (1–3). It is now also recognized that VDAC1 is involved in many physiological and pathophysiological processes, including Ca^{2+} homeostasis (2, 3), energy metabolism (1–5), and cell apoptosis (2– 4, 6 – 8).

Over the years, numerous proposals explaining the organization, structure, and transmembrane topology of VDAC1 have been offered. These proposals, guided by biochemical and biophysical findings (2, 9 –11) as well as by low resolution electron microscopy (EM), all showed VDAC1 to comprise 13–19 β-strands forming a β-barrel configuration around a cylindrical channel with a diameter of 20 –30 Å (12, 13). Recently, the topology and three-dimensional structure of recombinant human VDAC1 (hVDAC1) and murine VDAC1 (mVDAC1) were solved by NMR spectroscopy (14, 15) and x-ray crystallography (16). These studies revealed that VDAC1 adopts a β-barrel architecture, comprising 19 β-strands with a horizontally oriented α-helix N-terminal positioned midway within the pore. It should be noted that some concern about this structure has been expressed (17).

The existence of VDAC1 as oligomers has been demonstrated using various approaches. Purified and membrane-embedded mammalian VDAC1 were shown to assemble into dimers, trimers, tetramers, and higher oligomers by cross-linking using five different cross-linking reagents, findings later verified by fluorescence resonance energy transfer (FRET) analysis of purified VDAC1 labeled with FITC/EITC and reconstituted into liposomes (18). High resolution atomic force microscopy of purified native outer mitochondrial membrane from potato tubers (19) or yeast (20) showed VDAC to be distributed in an equilibrium of molecular states, ranging from single membrane-embedded pores to hexamers and high order oligomers (19), even extending to arrays containing up to 20 molecules (20). In addition, analysis using symmetry operators on the NMR-based structure of recombinant hVDAC1 implied the formation of a parallel dimer (14), whereas analysis of the crystal packing of mouse VDAC1 revealed an anti-parallel dimer that further assembles into hexamers (21). Despite these reported differences in the relative arrangement of human and mouse VDAC1 dimers, in both cases, the dimer interface is

[2] The abbreviations used are: VDAC, voltage-dependent anion channel; hVDAC1, mVDAC1, and rVDAC1, human, mouse, and rat VDAC1, respectively; BMOE, bis-maleimidoethane; EGS, ethylene glycol bis(succinimidylsuccinate); STS, staurosporine; DFDNB, 1,5-difluoro-2,4-dinitrobenzene; BRET2, bioluminescence resonance energy transfer.

TABLE 1

Oligonucleotides used for VDAC1 mutagenesis

Nucleotide substitutions leading to amino acid changes are in boldface type and underlined.

Substitution	Mutagenic primer	Template
I27R	Forward: AATAAAAC**G**TGATTTGAAAACGAAGTCCGAG Reverse: CAAATCA**C**GTTTTATTAAGCCAAAGCCG	rVDAC1
L29R	Forward: CACGGAG**GA** CACCAAAGTGAACGGCAGTCTG Reverse: CTTTTGGTG**TC** CTCCGTGTTGGCAGAACCTG	rVDAC1
S43L	Forward: GGAATTTACT**CT** CTCAGGTTCTGCCAACACGGAG Reverse: GTCCGAGAATGG**A**TTGGAATTTACT**CT**CTCAGGTTC	rVDAC1
T51D	Forward: GCTTGGTC**G**AGGACTGGAATTTCAAGC Reverse: CCAGTCCT**C**GACCAAGCTTGTGGCCAC	rVDAC1
L277R	Forward: CCTGGGC**GC**TGATGTGGACTTTG Reverse: CAAAGTCCACATCA**GC** GCCCAGG	rVDAC1
C127A	Forward: GTCGACCCTGATGCC**GC**CTTTTCGGCCAAAG Reverse: CTTTTGGCCGAAAAG**GC**GGCATCAGGGTCGAC	rVDAC1
L125R	Forward: ATCAACC**G**GGGCTGTGATGTGGACTTTGAC Reverse: CACAGCCC**C**GGTTGATATGCTCCCTCTTG	rVDAC1
C232A	Forward: CCACCC**TGT** TATGCCGATCTTGGCAAG Reverse: CGGCATAA**ACA** GGGTGGCACAGCCAT	rVDAC1
Q249L	Forward: GTACACTCT**G**ACCCTAAAACCAGGTATCAAACTG Reverse: GTCTAATTGGCTTAGGGTACACTCT**G**ACCCTA	rVDAC1
L29C	Forward: CACGGAG**TG**CACCAAAGTGAACGGCAGTCTG Reverse: CTTTTGGTG**CA**CTCCGTGTTGGCAGAACCTG	ΔCys-rVDAC1
T51C	Forward: GGTGAACAAGAAGTTGGAG**TG**TGCTGTCAATCTCGCC Reverse: GGCGAGATTGACAGCA**CA**CTCCAACTTCTTGTTCACC	ΔCys-rVDAC1
T204C	Forward: CAGGTCGACCCTGATT**GC**GCCTTTTCGGCC Reverse: GGCCGAAAAGGCG**CA**ATCAGGGTCGACCTG	ΔCys-rVDAC1
A231C	Forward: GCTTGGT**TGT** GGACTGGAATTTCAAGC Reverse: CCAGTCC**ACA** ACCAAGCTTGTGGCCAC	ΔCys-rVDAC1
L277C	Forward: GCTTGGT**TGT** GGACTGGAATTTCAAGC Reverse: CCAGTCC**ACA** ACCAAGCTTGTGGCCAC	ΔCys-rVDAC1

formed by β-strands 1, 2, 18, and 19 and potentially extends to include β-strands 3 and 4 (14, 21).

VDAC1 is now recognized to be a major regulator of mitochondria-mediated apoptosis, mediating the release of apoptotic proteins, such as cytochrome *c*, from mitochondria and interacting with pro- and anti-apoptotic proteins (2–4, 6–8, 22–25). Although it is accepted that multiple pathways and mechanisms of cytochrome *c* release can co-exist within a single model of cell death, depending on the cell type and the nature of the stimuli (26), the molecular architecture of the cytochrome *c*-conducting channel has yet to be determined. Previously, we proposed that VDAC1 oligomers function in apoptosis by forming a pore large enough to mediate the passage of cytochrome *c* (3, 18, 23, 25, 27, 28). Indeed, using chemical cross-linking, we demonstrated that the oligomeric assembly of VDAC1 in cultured cells is highly enhanced (up to 20-fold) upon induction of apoptosis by various agents (*e.g.* STS, curcumin, As_2O_3, etoposide, cisplatin, TNF-α, H_2O_2, UV irradiation, or VDAC1 overexpression), all of which act via mitochondria but through different mechanisms (28, 29). Moreover, when we employed bioluminescence resonance energy transfer (BRET2) to monitor VDAC1 oligomerization in living cells, we noted that incubation with apoptosis inducers enhanced the BRET2 signal, whereas exposure to apoptosis inhibitors prevented this enhancement (29). These findings support the hypothesis that VDAC oligomerization is involved in cytochrome *c* release and, therefore, in apoptosis.

In this study, site-directed mutagenesis, combined with cysteine substitution, chemical cross-linkers, and computational analysis, was employed in order to identify contact sites in the VDAC1 oligomer under physiological and apoptotic conditions. We identified two forms of dimeric VDAC1, one with a contact site involving β-strands 1, 2, and 19 and the second

involving β-strands 16 and 17. Moreover, the results suggest that VDAC1 exists as a dimer that undergoes conformational changes upon apoptosis induction to assemble into higher oligomeric states with contact sites also involving β-strand 8.

EXPERIMENTAL PROCEDURES

Materials—DL-Dithiothreitol (DTT), 1,5-difluoro-2,4-dinitrobenzene (DFDNB), EGTA, EDTA, leupeptin, phenylmethylsulfonyl fluoride (PMSF), sodium selenite, and staurosporine (STS) were obtained from Sigma. Monoclonal anti-VDAC antibodies raised to the N-terminal region of VDAC1 were purchased from Calbiochem-Novobiochem (Nottingham, UK). Ethylene glycol bis(succinimidylsuccinate) (EGS) and bis(maleimido)ethane (BMOE) were obtained from Pierce, and horseradish peroxidase (HRP)-conjugated anti-mouse antibodies were obtained from Promega (Madison, WI). Anti-actin antibodies were obtained from Santa Cruz Biotechnology, Inc. (Santa Cruz, CA), Dulbecco's modified Eagle's medium (DMEM) and the supplements, fetal calf serum, L-glutamine, and penicillin/streptomycin, were purchased from Biological Industries (BeitHaemek, Israel). Blasticidin was purchased from InvivoGen (San Diego, CA). Puromycin was purchased from ICN Biomedicals (Eschwege, Germany). siRNA was synthesized by Dharmacon (Lafayette, CO), from where the transfection reagent, DharmaFECT1, was also obtained.

Plasmids and Site-directed Mutagenesis—DNA encoding rVDAC1 (24) was cloned into the BamHI/NotI sites of the tetracycline-inducible pcDNA4/TO vector (Invitrogen). VDAC1 mutations were generated by PCR using the QuikChange mutagenesis method, using rVDAC1 or ΔCys-rVDAC1 (30) as cDNA templates (Table 1).

Cell Lines and Growth—T-REx-293 cells (HEK-293 cells that express the tetracycline repressor) were grown in DMEM, sup-

plemented with 10% fetal calf serum, 2 mM L-glutamine, 100 units/ml penicillin, 100 μg/ml streptomycin, 1 mM sodium pyruvate, and non-essential amino acids, and maintained in a humidified atmosphere at 37 °C with 5% CO_2. T-REx-293 cells stably expressing the pSUPERretro vector encoding shRNA-targeting hVDAC1 (hVDAC1-shRNA) and that showed a low (20–30%) level of endogenous hVDAC1 expression were grown with 0.5 μg/ml puromycin and 5 μg/ml blasticidin.

Cell Transfection—T-REx-293 cells were transiently transfected with plasmid pcDNA4/TO encoding native rVDAC1, mutated rVDAC1, or mutated ΔCys-rVDAC1 using calcium phosphate ($CaHPO_4$). Protein expression was induced by tetracycline (0.5–1.5 μg/ml) for 24–48 h.

For $CaHPO_4$-based transfection, cells (6×10^5) were seeded onto a 60-mm culture dish plate and grown in 3 ml of DMEM, supplemented with 10% fetal calf serum, 2 mM L-glutamine, 100 units/ml penicillin and 100 μg/ml streptomycin. Plasmid DNA (0.2–1.0 μg) was added to 250 μl of sterile $CaCl_2$ (240 mM) and mixed with 250 μl of sterile HEPES buffer (280 mM NaCl, 10 mM KCl, 1.5 mM $Na_2HPO_4 \cdot H_2O$, 12 mM glucose, 50 mM HEPES, pH 7.05, with NaOH). The mixture was applied to the T-REx-293 cells. Cells were maintained in a humidified atmosphere at 37 °C with 5% CO_2 for 16 h, at which time the medium was replaced with 3 ml of fresh medium.

VDAC1 Silencing and siRNA Transfection—Selective silencing of endogenous hVDAC1 was achieved using an shRNA-expressing vector. Nucleotides 483–501 of the hVDAC1 coding sequence were chosen as the target for shRNA specific to human VDAC1. The hVDAC1-shRNA-encoding sequence was created using the two complementary oligonucleotides indicated below, each containing the 19-nucleotide target sequence of hVDAC1 (nucleotides 483–501), followed by a short spacer and an antisense sequence of the target: Oligonucleotide 1, AGCTTAAAAAACACTAGGCACCGAGATT-ATCTCTTGAATAATCTCGGTGCCTAGTGTG; Oligonucleotide 2, GATCCACACTAGGCACCGAGATTATTCAAG-AGATAATCTCGGTGCCTAGTGTTTTTTA. The hVDAC1-shRNA-encoding sequence was cloned into the BglII and HindIII sites of the pSUPER retroplasmid (OligoEngine, Seattle, WA) containing a puromycin resistance gene. Transcription of this sequence by RNA-polymerase III produces a hairpin (hVDAC1-shRNA). Different clones of T-REx cells expressing low level of endogenous VDAC1 were scanned. Clone C4, showing the highest reduced VDAC1 expression (30% of the level in non-treated cells; see Fig. 2C), was selected and used.

For VDAC1 silencing by siRNA, T-REx-293 cells were seeded into 6-well plates (2.5×10^5 cells/well). After 24 h, cells were transfected with human hVDAC1-directed siRNA (25 nM) using DharmaFECT1 transfection reagent, according to the manufacturer's instructions (Darmacon).

Chemical Cross-linking—Control T-REx 293 cells or T-REx 293 cells transfected to express native, mutated rVDAC1 or mutated ΔCys-rVDAC1 (3 mg/ml) were cross-linked by incubation with different concentrations of EGS (50–300 μM) or DFDNB (100–200 μM) in PBS, pH 8.3 (15–30 min, 30 °C), and the reaction was stopped by adding SDS-PAGE sample buffer. For cross-linking with BMOE, cells were incubated with the reagent (0.1–1 mM) in PBS, pH 7.2, at 30 °C, and after 30 min, the reaction was terminated by adding DTT (10 mM). Samples (30 μg) were subjected to SDS-PAGE and immunoblotting using anti-VDAC antibodies. Protein concentrations were determined with the Lowry method, using BSA as a standard.

Gel Electrophoresis and Immunoblot Analysis—SDS-PAGE was performed according to Laemmli (31). Gels were stained with Coomassie Brilliant Blue or electrotransferred onto nitrocellulose membranes for immunostaining. Membranes containing the transferred proteins were blocked with 5% nonfat dry milk and 0.1% Tween 20 in Tris-buffered saline and then incubated with monoclonal anti-VDAC1 antibodies (1:10,000), followed by incubation with HRP-conjugated anti-mouse IgG secondary antibodies (1:10,000). An actin-specific polyclonal antibody (1:10,000) was used as a loading control. After treatment with the appropriate primary and secondary antibodies, enhanced chemiluminescence (Pierce) was performed. Quantitative analysis of the bands was carried out using EZQuant-Gel one-dimensional software analysis according to parameters defined by the software algorithms for band and lane depiction.

Identification of Weakly Stable Regions by Computational Modeling—The empirical energy for each of the 19 VDAC1 β-strands from the crystal structure was calculated using the statistical mechanics model described in Ref. 32. Briefly, the energy for each residue consists of two terms. First, each residue is assigned an energy value of burying this residue at the particular depth in the lipid bilayer and with the orientation of its side chain, as seen in the crystal structure. There are two possible side chain orientations, namely facing the lipid environment or facing inside the barrel. This value is called the "single body term." Second, each residue interacts with two residues on separate neighboring strands through strong backbone hydrogen bond interactions, side chain interactions, and weak hydrogen bond interactions, which collectively make up the two-body energy term. Strand energy is the summation of both single body and two-body energy terms over all residues in the β-strand. Those strands with energy higher than the mean energy of all the strands were regarded as weakly stable. To identify the most unstable residue in a strand, we calculated the empirical energy required to insert that residue at its proper depth in the lipid bilayer with the corresponding side chain orientation (single body term), as seen in the crystal structure. The residues that required relatively high empirical energy to insert into the lipid bilayer were termed as weakly stable residues. The empirical energy function (TmSIP) used is derived from bioinformatics analysis of β-barrel membrane proteins (32–34). Those strands with energy higher than the mean energy of all of the strands were regarded as weakly stable. Because TM β-barrels are diverse, the mean energy value varies, and there is no strict universal cut-off value.

RESULTS

To identify the interfaces between VDAC1 molecules in the oligomeric states under physiological and apoptotic conditions, we performed computational analysis, combined with site-directed mutagenesis and cysteine substitution and chemical cross-linking. Together, these approaches enabled us to map out possible interfaces between VDAC1 molecules.

A

B
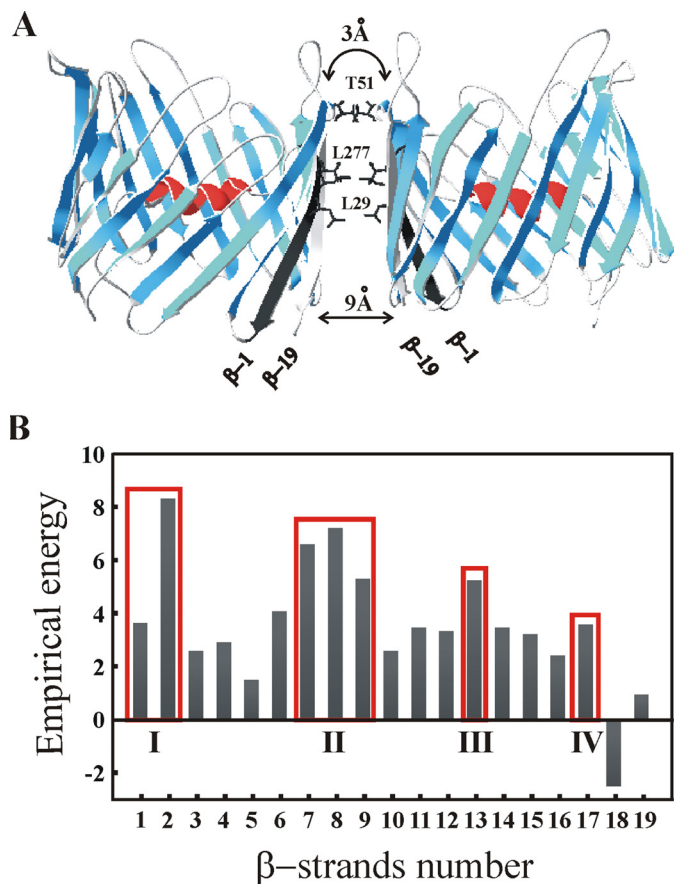
FIGURE 1. Proposed three-dimensional structure of a VDAC1 dimer and the computational stability profile of VDAC1 transmembrane β-strands. *A*, ribbon representation of the NMR-based hVDAC1 dimer structure (14). The proposed strands involved in dimerization are marked (*β*1 and *β*19), with residues at the dimer interface annotated. The distance between the monomers is 3 Å at the cytoplasm-facing side and 9 Å at the intermembrane space-facing side. *B*, empirical energy values of the 19 β-strands of VDAC1. There are four unstable regions in VDAC1. Strands 1 and 2 comprise the first unstable region (*I*). Strands 7–9 form the second region (*II*). Strands 13 and 17 form the third (*III*) and fourth (*IV*) unstable regions, respectively.

Structure- and Computation-based Selection of Predicated VDAC1 Dimerization Site—It has been proposed that the interface in a VDAC1 dimer involves amino acid residues located in β-strands 1, 2, 18, and 19 from both VDAC1 monomers (14, 21), as depicted in Fig. 1*A*. In addition to this structural prediction, we performed bioinformatics analysis based on a recent study in which weakly stable regions were computationally identified in β-barrel membrane proteins. It was found that these weakly stable regions strongly indicate the existence of protein-protein interaction sites. Using 25 β-barrel membrane proteins, the oligomeric state of each protein was predicted correctly, and the protein-protein interaction interfaces were recovered at an accuracy of 78% (32).

The calculated oligomerization index (32) of 2.47 corresponds to a value in the range where both monomeric and oligomeric β-barrel proteins have been observed. Although the analysis presented in Ref. 32 was based on bacterial TM β-barrels, we assume that it is applicable to mitochondrial proteins. This is reasonable, because the outer membrane insertion recognition machineries of bacteria and mitochondrial β-barrel membrane proteins are interchangeable (33, 34), and they share

a similar evolutionary pattern (35). Therefore, we conclude that VDAC1 probably forms transient oligomers.

β-strands with energy value higher than the mean value (3.53 for VDAC1) were predicted to be weakly stable. Weakly stable regions often signal the existence of an oligomer, because the strands located in the interface of protein-protein interactions are considerably less stable without their interaction partners. There are four unstable regions in VDAC1. Strands 1 and 2 comprise the first unstable region (I); strands 7–9 form the second region (II); and strands 13 and 17 form the third (III) and fourth (IV) unstable regions, respectively (Fig. 1*B*).

Identifying VDAC1 Dimerization Site—To verify the involvement of the region that includes β-strands 1, 2, and 19 (*i.e.* the first unstable region) in VDAC1 oligomerization, we replaced amino acids in rVDAC1 β-strand 1 (Ile-27 and Leu-29), in the β-2-β-3 connecting loop (Thr-51), and in β-strand 19 (Leu-277) with arginine or aspartate in order to interfere with VDAC1 oligomerization.

To monitor the effects of these mutations on VDAC1 oligomerization, we expressed the mutated rat (r)VDAC1 proteins, I27R-, L29R-, T51D-, or L277R-VDAC1, in cells presenting low levels of endogenous hVDAC1 (30% of non-treated cells). Low levels of hVDAC1 were achieved either using cells stably expressing hVDAC1-shRNA (clone C4; Fig. 2*C*) or by introducing hVADC1-siRNA, both of which do not interfere with the expression of rVDAC1. These T-REx-293 cells expressing native or mutated rVDAC1 were treated with STS to induce apoptosis. Cells expressing either native rVDAC1 or one of the mutant rVDAC1s (*i.e.* I27R-, L29R-, T51D-, or L277R-rVDAC1) were incubated with the cell-permeable cross-linker, EGS, and immunoblotted with anti-VDAC1 antibodies to reveal the profile of VDAC1 oligomers formed (Fig. 2*A*).

Wild type and mutant rVDAC1 were expressed at the same level, albeit at levels 7-fold over the level in cells whose expression was silenced using specific siRNA (decreased by 70%) and ~2-fold higher than that of endogenous hVDAC1 (Fig. 2*A*, *low exposure panel*). The results showed that, compared with native rVDAC1 amounts, the levels of dimers and higher oligomeric forms of VDAC1 were greatly reduced (up to 95% decrease; Fig. 2*A*, *high exposure panel*) in cells expressing the I27R, L29R, and T51D mutations in β-strands 1 and 2 and in the L277R mutant in β-strand 19. Thus, substitution of non-polar residues at positions assigned to the dimerization interface and facing the lipid bilayer with either positively or negatively charged amino acids interfered with VDAC1 oligomerization.

In the case of wild type rVDAC1, high VDAC1 expression levels (2.3-fold increase; Fig. 2*A*, *low exposure panel*) shifted the equilibrium of VDAC1 organization toward the formation of oligomers, even without induction of apoptosis (Fig. 2*A*). Indeed, we recently demonstrated that VDAC1 overexpression is associated with rVDAC1 oligomerization (25). Accordingly, although the expression level of native rVDAC1 is similar to that of mutated rVDAC1, the expressed native but not mutated VDAC1 shifted the equilibrium from the monomeric to the oligomeric state.

It is also of note that interrupting rVDAC1 dimerization also disrupted formation of all higher oligomeric states (*i.e.* trimers,
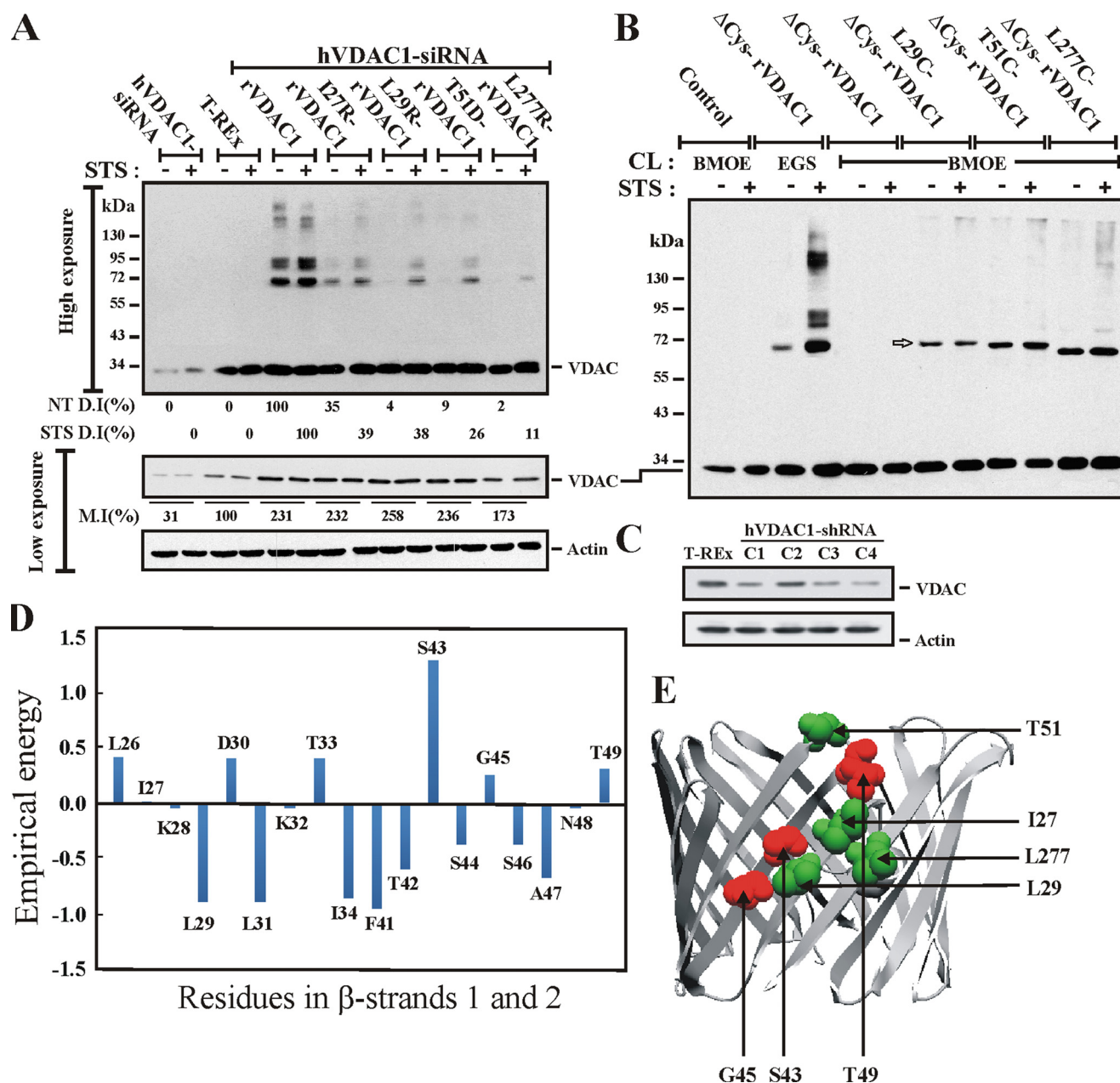
FIGURE 2. **Mutations and cysteine substitution introduced at VDAC1 positions at the predicted dimerization site and empirical energy analysis point to β strands 1, 2, and 19 as being proximal in dimeric VDAC1.** *A*, native rVDAC1 and mutated I27R-, L29R-, T51D-, or L277R-rVDAC1 were expressed upon induction by tetracycline (1.5 μg/ml, 24 h) in T-REx-293 cells treated with siRNA to reduce the expression level of endogenous hVDAC1, as described under "Experimental Procedures." 24 h post-induction, the cells (3 mg/ml), either treated or not with STS (3.5 μM, 4 h), were washed and incubated with the cross-linker reagent, EGS (50 μM), for 15 min at 30 °C, subjected to SDS-PAGE (10% acrylamide), and immunoblotted using N terminus-specific anti-VDAC1 antibodies. The detection films were also subjected to low exposures to demonstrate the low level of hVDAC1 in the siRNA-treated cells as well as the similar expression levels of rVDAC1 in cells transfected with various plasmids. Quantitative analysis of band intensities of monomer (*M.I.*) and dimer (*D.I.*) in control samples (−*STS*) and in samples treated with STS (+*STS*) is also shown. *B*, T-REx-293 cells stably expressing hVDAC1-shRNA (clone C4 in *C*) were transfected to express ΔCys-rVDAC1 or ΔCys-rVDAC1 mutants (L29C, T51C, and L277C) and treated with STS (3.5 μM, 4 h). 24 h after induction of expression with tetracycline (1.5 μg/ml), cells were incubated at 30 °C with the thiol-specific cross-linking reagent (*CL*), BMOE (100 μM), for 30 min or with EGS (50 μM) for 15 min. Cells were subjected to SDS-PAGE (10% acrylamide) and immunoblotting using N terminus-specific anti-VDAC1 antibodies or anti-actin antibodies as loading control. The positions of molecular mass protein standards are indicated. The *arrow* indicates the different mobility of the mutated VDAC-containing adducts at the dimer position. *C*, the VDAC1 expression levels of T-REx-293 cells and different clones stably expressing hVDAC1-shRNA are shown. Clone C4 was used as hVDAC1-shRNA cells. *D*, the contribution of residues in the transmembrane domains of β-strands 1 and 2 to overall stability, as revealed by empirical energy analysis. *E*, the spatial positions of Ser-43, Gly-45, and Thr-49 (*red*), with respect to Ile-27, Leu-29, Thr-51, and Leu-277 (*green*).

tetramers, etc.) (Fig. 2*A*). This suggests that dimerization is the first obligatory step leading to VDAC1 oligomerization.

Next, we examined the contribution of amino acid residues in the transmembrane domain to VDAC1 oligomerization based on the depth of each amino acid in the bilayer and the orientation of its side chain. This computational analysis revealed that β-strand 2 is the most unstable strand, with residue Ser-43 in β-strand 2, facing the lipid phase, predicted to be the most unstable residue in the protein-protein interaction interface and probably stabilized by protein-protein interac-
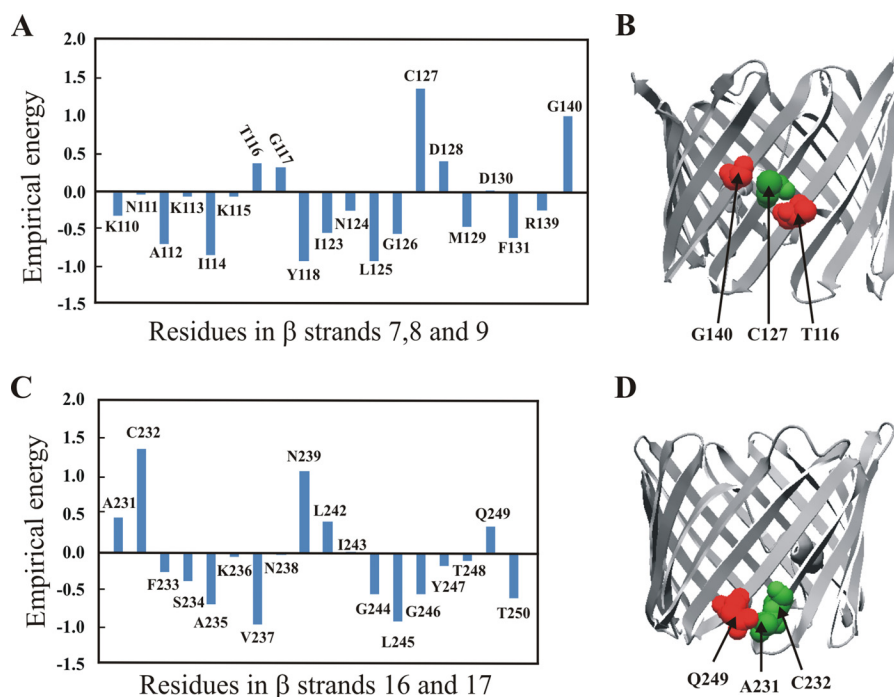
FIGURE 3. **VDAC1 cysteine residues, Cys-127 and Cys-232, are the most unstable residues in the second and the fourth unstable regions.** *A*, the contribution of amino acid residues in the transmembrane domains of β-strands 7–9 to the overall stability of these strands. Thr-116, Cys-127, and Gly-140 are unstable residues facing the bilayer. *B*, the spatial positions of Thr-116 (*red*) in β-strand 7, Cys-127 (*green*) in β-strand 8, and Gly-140 (*red*) in β-strand 9, forming the second unstable region. *C*, contribution of amino acid residues in the transmembrane domains of β-strands 16 and 17 to the overall stability of these strands. *D*, residues Ala-231 (*green*), Cys-232 (*green*) in β-strand 16, and Gln-249 (*red*) in β-strand 17 are in close proximity in the fourth unstable region.

tions (Fig. 2*D* for empirical energy values for all of the residues facing lipids in β-strands 1 and 2). Moreover, the spatial position of Ser-43 places it in close proximity to Ile-27 and Leu-29 (Fig. 2*E*), consistent with the experimental observations.

To further identify VDAC1 dimerization sites, we replaced selected amino acids with cysteine residues and subsequently performed cross-linking with the thiol-specific cross-linking reagent BMOE. WT rVDAC1 contains two cysteine residues, Cys-127 and Cys-232, which, according to the three-dimensional VDAC1 structure and membrane topology map, face the lipid interface and the internal pore, respectively (14–16). Therefore, we first constructed a cysteineless version of rVDAC1, ΔCys-rVDAC1, by replacing both Cys-127 and Cys-232 with alanine residues (*i.e.* (C127A/C232A)-rVDAC1). We then inserted a cysteine residue into ΔCys-rVDAC1 at strategic locations and performed cross-linking with BMOE. The formation of rVDAC1 cross-linked products was subsequently analyzed by immunoblotting with anti-VDAC1 antibodies.

Exposure of cells expressing ΔCys-rVDAC1 to BMOE resulted in no cross-linking products (Fig. 2*B*), indicating that the reagent is specific for thiol groups. EGS, unlike BMOE, reacts with primary amines and produced dimers and other VDAC1-containing cross-linked products in cells expressing ΔCys-rVDAC1 (Fig. 2*B*). Cysteine substitution L29C (β-strand 1), T51C (in the loop connecting β-strands 2 and 3), or L277C (β-strand 19) in ΔCys-rVDAC1 allowed the formation of dimers, stabilized by BMOE (Fig. 2*B*). These findings suggest that positions Leu-29, Thr-51, and Leu-277 are close enough within a VDAC1 dimer to allow BMOE (8 Å length) to cross-react with cysteine residues located at these positions in each of two VDAC1 molecules composing the dimer. Interestingly, the

L277C-ΔCys-rVDAC1 BMOE-cross-linked dimer was found to migrate with lower mobility than the EGS-cross-linked ΔCys-rVDAC1 dimer or the BMOE-cross-linked L29C- or T51C-ΔCys-rVDAC1 dimers (Fig. 2*B*).

In contrast, in VDAC1 containing a single cysteine residue (Cys-127) in β-strand 8 or a cysteine substitution at Thr-204 in β-strand 14 (*i.e.* T204C-ΔCys-rVDAC1), no dimers were formed with BMOE (see Fig. 4, *A* and *B*), suggesting that within a VDAC1 dimer under physiological conditions, β-strands 8 and 14 from two VDAC1 molecules are not in close enough proximity to permit BMOE cross-linking.

Probing of Cysteine Residues of Wild Type VDAC1 Leads to Identification of Second VDAC1 Dimerization Site—VDAC1 trimer, tetramer, hexamer, and higher oligomer formation requires more than a single contact site between VDAC1 monomers. After verifying the involvement of the first unstable region in dimer formation (see Fig. 1*B*), we considered additional unstable regions. In the second unstable region, composed of β-strands 7–9, there are three unstable residues, namely Thr-116 in β7, Cys-127 in β-strand 8, and Gly-140 in β-strand 9 (Fig. 3*A*). Moreover, these three residues are spatially located in the same region (Fig. 3*B*) and may form an association site. Of these, Cys-127 is the most important because it is the most unstable residue of the three (Fig. 3*A*). Although Gly-117, Asp-128, and Val-143 are also unstable, their side chains face inside the β-barrel and are not likely to be involved in protein-protein interactions.

The third unstable region calculated is centered on β-strand 13. The instability of this strand stems from two modestly unstable residues, Gly-192 and Gln-196. The crystal structure of VDAC1 (Protein Data Bank code 3EMN) shows a lipid bound
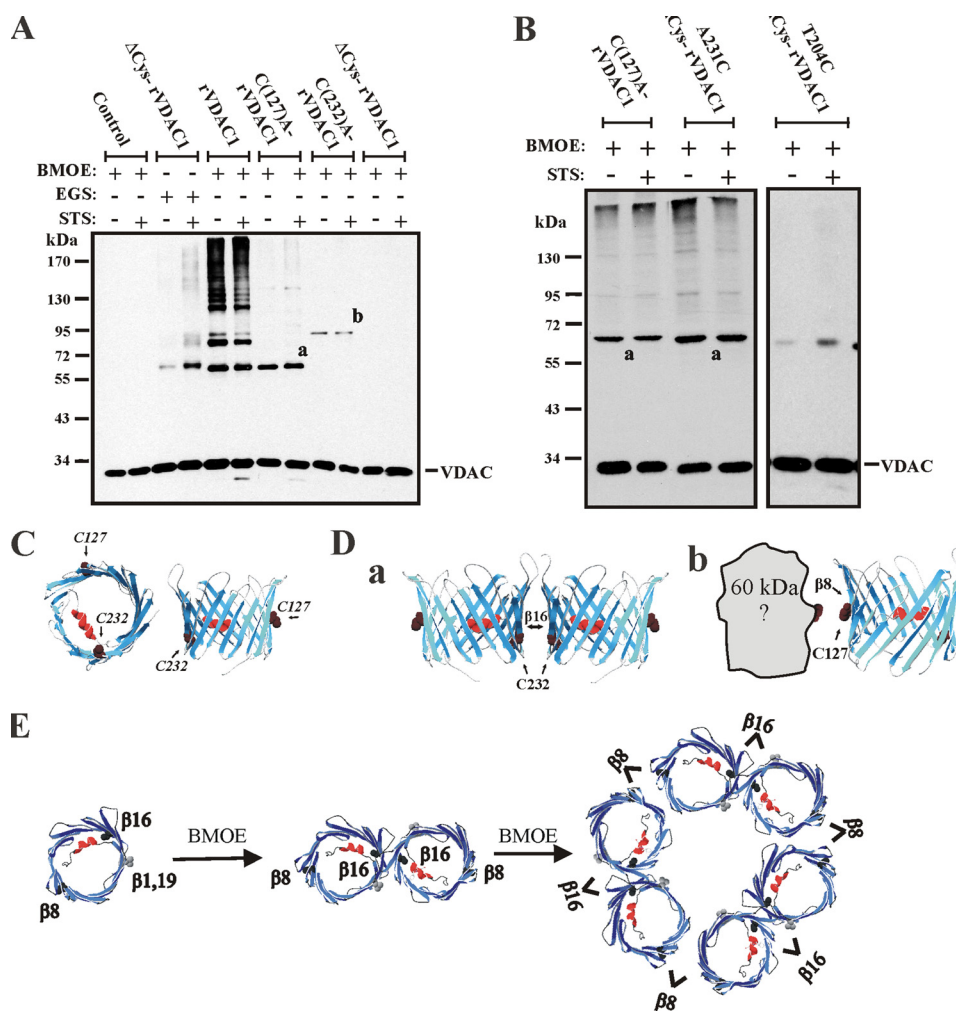
FIGURE 4. **Cross-linking with BMOE reveals a possible VDAC1 oligomerization site and interaction site with an associated protein.** T-REx-293 cells, stably expressing hVDAC1-shRNA, were transfected to express rVDAC1 or C127A-, C232A-, or ΔCys-rVDAC1 (*A*) or C127A-, A231C-ΔCys-, or T204C-ΔCys-rVDAC1 (*B*). 24 h after induction of expression with tetracycline (1.5 μg/ml), the cells were treated with STS (3.5 μM, 4 h). Cells were incubated with BMOE (100 μM) for 30 min at 30 °C and subjected to SDS-PAGE (10% acrylamide) and immunoblotting using N terminus-specific anti-VDAC1 antibodies. *a* and *b* adjacent to the immunoreactive bands indicate the proposed VDAC1 oligomerization state, as illustrated in *D*. *C*, a schematic representation of hVDAC1 with the proposed (14–16) orientation of its cysteine residues shown, with respect to the bilayer and the pore. *D*, a proposed VDAC1 dimeric state (*a*) and a heterodimer formed with a protein of a predicted mass of 60 kDa (*b*). *E*, proposed model for BMOE-induced conformational change. Cross-linking of β-strands 16 by BMOE induces conformational changes in the VDAC1 dimer that allow further cross-linking of β-strand 8 to form higher oligomeric forms.

to Gly-192, suggesting that this weakly stable region may be stabilized by protein-lipid interactions, a known mechanism that is also observed in the structure of FhuA (36, 37). Because we speculate that such modification does not have a dominant effect on the oligomerization of VDAC1, it was not experimentally addressed.

The fourth unstable region consists of β-strand 17, which is locally unstable and is found right next to the most stable β-strand (β-strand 18; see Fig. 1*B*) in the protein. It is possible that β-strand 18 stabilizes the relatively unstable β-strand 17. Specifically, unstable Gln-249 (Fig. 3*C*) in β-strand 17 is found in spatial proximity to Cys-232 and Ala-231 (Fig. 3*D*), residues that are the most unstable in β-strand 16 (Fig. 3*C*); all may play an important role in oligomerization.

Considering the fact that the VDAC1 cysteine residues, Cys-127 and Cys-232, are the most unstable positions in the second and the fourth unstable regions, respectively, we probed these residues to further explore VDAC1 oligomerization sites.

In addition to ΔCys-rVDAC1-expressing cells, we constructed single cysteine-encoding (C127A or C232A)-rVDAC1 constructs and exposed the transformed cells to BMOE (Fig. 4). When native rVDAC1, which contains two cysteine residues (Cys-127 and Cys-232), was exposed to BMOE, we obtained several rVDAC1-containing cross-linking products at the levels of dimers, trimers, tetramers, hexamers, and other higher molecular masses (Fig. 4*A*; see also Fig. 6*A*). This suggests that both the second and the fourth unstable regions that contained these cysteine residues are in close proximity and allowed cross-linking with BMOE. Furthermore, the presence of rVDAC1-containing bands corresponding to higher molecular moieties, most probably corresponding to hetro-oligomeric states of VDAC1 (according to their apparent molecular masses), suggests that VDAC1 associates with other protein(s) via one or both of its cysteine residue-containing unstable regions. Because one of the VDAC1 cysteine residues is thought to face the pore, whereas the other is exposed to the lipid phase

(14–16), the interacting proteins could be membranal, cytosolic, or located within the intermembrane space.

When C127A-rVDAC1 (containing a single cysteine, Cys-232 in β-strand 16) was exposed to BMOE, dimers were obtained (Fig. 4*A*), suggesting that within the rVDAC1 dimer, the two Cys-232 residues face each other and are in close proximity (<8 Å) (Fig. 4*C*, *a*). Thus, although Cys-232 in β-strand 16 is predicted to face the channel pore (Fig. 4*B*), according to recent VDAC1 topology models (14–16), our results suggest that this residue can also face the lipid phase, allowing dimer formation. The fact that Cys-232 is a very unstable residue in β-strand 16 (see Fig. 3*B*) supports the idea that it can change its orientation toward the lipid phase. Therefore, the second unstable VDAC1 region may serve as part of another VDAC1 contact site (see Fig. 7).

Furthermore, introducing a cysteine residue into β-strand 16, as in the A231C-ΔCys-rVDAC1 mutant, allowed formation of a dimer (stabilized by BMOE) with the same mobility as C232-rVDAC1 (Fig. 4*B*). These results taken together suggest that both Ala-231 and Cys-232 are in the proximity of a protein-protein interaction interface but are not necessary the residues that form the interaction site. This is also supported by our computational analysis that predicts Gln-249, a spatial neighbor of Ala-231 and Cys-232 (see Fig. 3*D*), to be unstable and thus more likely to be involved in protein-protein interactions.

However, when C232A-rVDAC1 (containing a single cysteine residue, Cys-127 in β-strand 8) was expressed, no dimers were obtained upon exposure to BMOE (Fig. 4*A*), suggesting that Cys-127 in β-strand 8 is not found in the contact site responsible for the formation of dimeric VDAC1.

In addition, the mutation C232A has a stabilizing effect on the fourth unstable region of VDAC1 comprising β-strands 16 and 17 (data not shown). Thus, stabilization may reduce the ability of the protein to form oligomers.

Finally, in cells expressing C232A-rVDAC1, a minor anti-VDAC1 antibody-reacting protein band with a mobility of 90 kDa was observed (Fig. 4*A*). This band probably represents VDAC1 cross-linked with a 60-kDa protein of unknown identity (Fig. 4*D*, *b*).
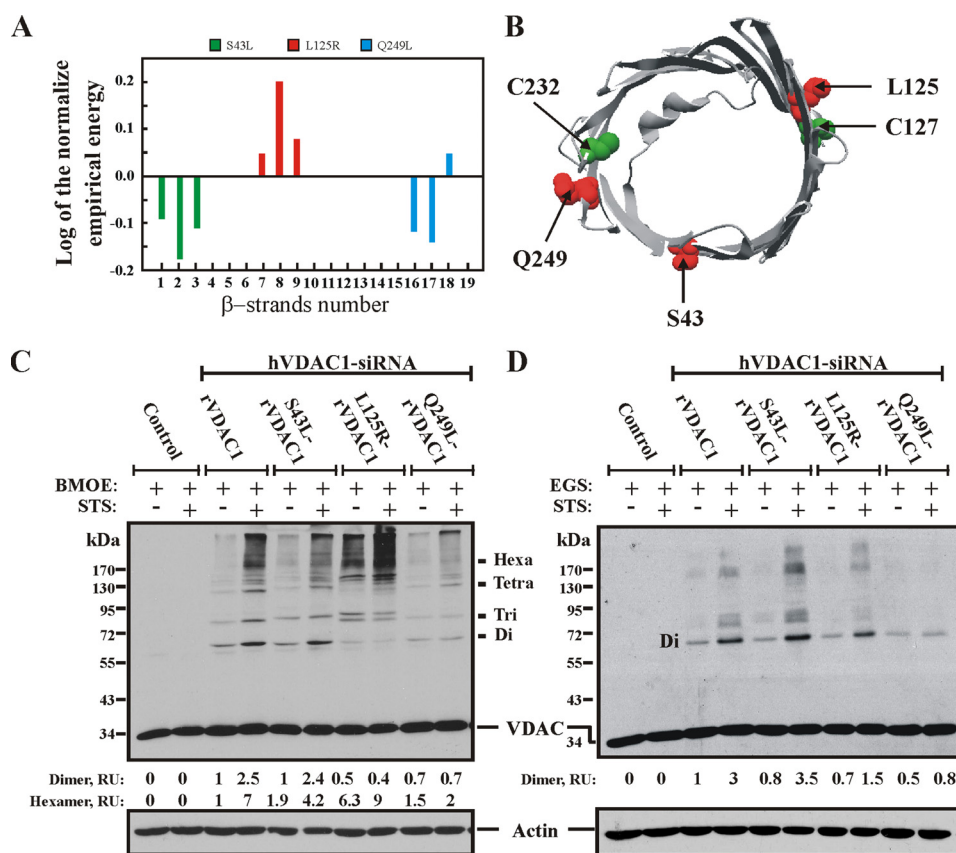
Stabilizing and Destabilizing Mutations in Second and Fourth Unstable Regions Change VDAC1 Oligomerization State— Computational analysis of the contribution of individual residues in the transmembrane domains of VDAC1 to the overall stability of the β-strands can predict mutations that stabilize or destabilize the protein and thus affect the oligomeric state. Accordingly, we replaced the unstable residues Ser-43 in β-strand 2 and Gln-249 in β-strand 17 with the stabilizing leucine side chain. In addition, we replaced the stable residue, Leu-125 in β-strand 16, with the unstable arginine side chain. Fig. 5*A* shows the calculated empirical energy values of the 19 β-strands of VDAC1. The normalized log ratio of the empirical energy of the selected mutation with respect to the native residue shows the local stabilizing and destabilizing effects of each mutation. The spatial positions of Ser-43, Leu-125, Cys-127, Cys-232, and Gln-249 are shown in Fig. 5*B*. Leu-125 and Gln-249 are in close proximity to Cys-127 and Cys-232, whereas Ser-43 is not close to either of these VDAC1 cysteine residues.

Next, we monitored the effects of these mutations on VDAC1 oligomerization by expressing the mutant rVDAC1 proteins, S43L-, L125R-, and Q249L-rVDAC1, in cells presenting low levels of endogenous hVDAC1. These T-REx-293 cells, expressing wild type or mutated rVDAC1, were treated with STS to induce apoptosis, subjected to cross-linking with EGS or BMOE, and immunoblotted with anti-VDAC1 antibodies to reveal the profile of VDAC1 oligomers formed.

Mutation S43L showed the same oligomerization pattern as native rVDAC1, with either EGS or BMOE (Fig. 5, *C* and *D*). On the other hand, the BMOE cross-linker revealed that the destabilizing mutation, L125R, reduced the dimer band (~50% less relative to untreated rVDAC1; Fig. 5*C*) while increasing the level of higher VDAC1-containing oligomers (1.3–6-fold increase in the intensity of the hexamer band; Fig. 5*C*). This was particularly true for the 90-kDa protein band that was obtained with C232A-rVDAC1 (see Fig. 4, *A* and *C*, *b*). VDAC1 oligomerization was also obtained with the less specific cross-linker, EGS (Fig. 5*D*). These results suggest that the mutated L125R-rVDAC1 is unstable in the monomeric form and thus undergoes stabilization via oligomerization to form higher oligomer forms, with few dimeric species formed.

As expected, the stabilizing mutation, Q249L, in comparison with rVDAC, reduced the VDAC1 oligomerization level (~40% less, relative to rVDAC1; Fig. 5, *C* and *D*), as revealed by cross-linking with either EGS or BMOE (Fig. 5, *C* and *D*). These results suggest that the stable Q249L-rVDAC1 monomer has a lower tendency to form oligomers.

VDAC1 Undergoes Conformational Changes upon Apoptosis Induction—The enhanced VDAC1 oligomerization observed when apoptosis was induced with STS and using EGS as cross-linker (16.1 Å length) to stabilize VDAC1 oligomers was not observed when BMOE (8-Å length) was used (Figs. 2*B* and 4*A*), suggesting that cross-linker length explains this observation. To test this assumption, T-REx-293 cells stably expressing hVADC1-shRNA were transfected to express rVDAC1, treated with STS, and then subjected to cross-linking with the primary amine-reactive cross-linker EGS (16.1 Å length) or DFDNB (3 Å length) or with the thiol-specific cross-linker BMOE (8-Å length). VDAC1 oligomeric forms, as revealed by immunoblotting with anti-VDAC1 antibodies, showed an increase in amount when apoptosis was induced with STS and EGS but not when BMOE or DFDNB was used to stabilize the VDAC1 oligomers formed (Fig. 6*A*). Identical cross-linking patterns were obtained with BMOE and DFDNB, before and after apoptosis induction, with a pattern appearing to resemble that resulting from cross-linking with EGS after the induction of apoptosis (Fig. 6*A*, *black rectangle*). These findings may result from differences in cross-linker lengths and flexibility as well as from VDAC1 conformational changes that occur upon apoptosis induction, as discussed below. Apoptosis induced by STS or selenite treatment not only enhanced VDAC1 oligomerization but also resulted in the appearance of an anti-VDAC1 antibody-reactive band corresponding to monomeric VDAC1 with modified electrophoretic mobility (Fig. 6*B*, *white arrow*).

FIGURE 5. **Effects of stabilizing and destabilizing mutations at β-strands 8 and 17 on VDAC1 oligomerization.** *A*, the normalized empirical energy values of 19 VDAC1 β-strands after the mutagenesis of S43L, L125R, and Q249L (shown on a logarithmic scale). Normalization was performed with the energy value determined for the wild type protein, defined as zero. Mutations S43L and Q249L reduce the energy and stabilize the monomer, whereas L125R increases the energy and, thereby, destabilizes the monomers, leading to oligomerization. *B*, the spatial positions of Ser-43 (*red*) in β-strand 2, Leu-125 (*red*), and Cys-127 (*green*) in β-strand 8 and Cys-232 (*green*) and Gln-249 (*red*) in β-strands 16 and 17, respectively. Leu-125 and Gln-249 are in close proximity to Cys-127 and Cys-232, respectively, whereas Ser-43 is not close to either of the VDAC1 cysteine residues. *C* and *D*, native rVDAC1 and mutated S43L-, L125R-, or Q249L-rVDAC1 were expressed upon induction by tetracycline (1.5 μg/ml, 24 h) in T-REx-293 cells treated with siRNA to express a low level of hVDAC1, as described under "Experimental Procedures." 24 h postinduction, cells (3 mg/ml) either treated or not with STS (3.5 μM, 4 h) were incubated at 30 °C with the thiol-specific cross-linking reagent, BMOE (100 μM), for 30 min (*C*) or with EGS (50 μM) for 15 min (*D*). Cells were subjected to SDS-PAGE (10% acrylamide) and immunoblotting using N terminus-specific anti-VDAC1 antibodies or anti-actin antibodies as loading control. The positions of molecular mass protein standards are indicated. Quantitative analysis of dimer and hexamer band intensity, as -fold change from that seen in cells expressing wild type rVDAC is also presented.

DISCUSSION

In this study, we analyzed contact sites in VDAC1 dimers and higher oligomers under physiological and apoptotic conditions using computational modeling and experimental approaches. Based on bioinformatics analysis, four contact sites between VDAC1 molecules were proposed and then confirmed using site-directed mutagenesis and cysteine replacement combined with chemical cross-linking. The results also suggest that VDAC1 exists in equilibrium between monomers and dimers that undergo conformational changes upon apoptosis induction to assemble into higher oligomeric states.

Dissection of First VDAC1 Oligomerization Sites—X-ray crystallography of hVDAC1 suggested the formation of a parallel dimer (14), whereas analysis of the crystal packing of mVDAC1 revealed an anti-parallel dimer, which further assembles into hexamers (21). In both cases, the dimer interface was proposed to be formed by β-strands 1, 2, 18, and 19, extending potentially to β-strands 3 and 4.

Our bioinformatics analysis (32) predicts that VDAC1 contains four unstable regions. Strands 1 and 2 comprise the first unstable region, strands 7–9 form the second region, and

strands 13 and 17 form the third and fourth unstable regions, respectively. These unstable regions often signal the existence of an oligomer and may be located in the protein-protein interaction interface (32).

To experimentally probe the domains in rVDAC1 involved in VDAC1 dimerization or oligomerization, a series of mutations were introduced into rVDAC1, and the effects of these mutations on VDAC1 oligomeric status were analyzed. When residues in β-strands 1, 2, and 19 were mutated (*i.e.* I27R or L29R from β-strand 1, T51D from β-strand 2, L277R from β-strand 19), VDAC1 oligomerization was highly reduced, suggesting that these residues are found at the interface between two VDAC1 monomers in the oligomeric states (Fig. 2*A*). Replacement of arginine or aspartate at the equivalent positions in ΔCys-rVDAC1 with a cysteine residue allowed dimer formation (Fig. 2*B*), providing further support for the proposed location of these residues at the dimer interface. These results are consistent with previous structural findings showing that the VDAC1 dimer interface is formed by β-strands 1, 2, 18, and 19 (14, 21). This site was also predicted by our computational analysis, which points to Ser-43 as being very unstable. The I27R
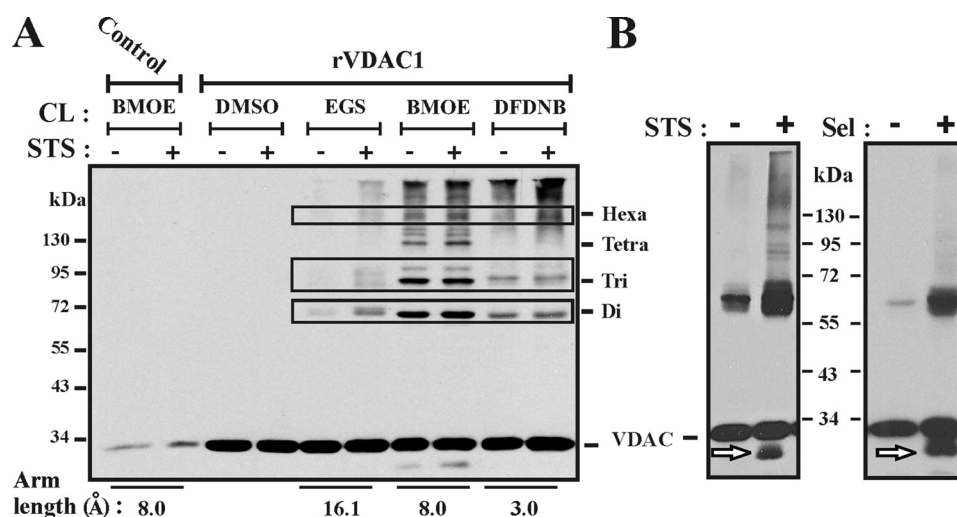
FIGURE 6. **The long cross-linker EGS but not the shorter reagents, DFDNB and BMOE, reveals increases in VDAC1 oligomerization and that VDAC1 undergoes conformational changes upon apoptosis induction.** *A*, T-REx-293 cells stably expressing hVDAC1-shRNA (low hVDAC1 level) were transfected to express rVDAC1. 24 h after expression induction by tetracycline (1.5 μg/ml), the cells were treated with STS (3.5 μM, 4 h). These were then incubated at 30 °C with the thiol-specific cross-linking reagent BMOE (100 μM) or with the amine reactive cross-linker EGS (50 μM) or DFDNB (100 μM). Samples were subjected to SDS-PAGE (10% acrylamide) and immunoblotting using N terminus-specific anti-VDAC1 antibodies. VDAC-containing dimers (*Di*), trimers (*Tri*), tetramers (*Tetra*), and hexamers (*Hexa*) and the positions of molecular weight protein standards are provided. The *black rectangles* show the similar oligomerization patterns obtained with the three different cross-linkers. The increase in VDAC1 oligomerization upon apoptosis induction is seen only with the long cross-linker, EGS (16.1 Å) and not with either of the short cross-linkers, BMOE (8 Å) or DFDNB (3 Å). *B*, T-REx-293 cells were treated with STS (3.5 μM, 4 h) or selenite (25 μM, 4 h) and incubated with EGS (300 μM). The enhanced VDAC1 oligomerization and appearance of intramolecular cross-linked monomers upon apoptosis induction are indicated by the *white arrow*.

and L29R mutations found to reduce oligomerization (Fig. 2) may provide Ser-43 with stabilizing interactions, which would, in turn, reduce the tendency of the mutant proteins to participate in protein-protein interactions. In contrast, with VDAC1 containing a single cysteine (*i.e.* Cys-127 in β-strand 8 (Fig. 3*A*) or Cys-204 in β-strand 14 (Fig. 4*D*)), no dimers or oligomers were obtained upon cross-linking with BMOE, suggesting that β-strands 8 and 14 are not located at the interface between two VDAC molecules in a dimer. Thus, we propose a possible spatial arrangement and orientation of the two VDAC1 monomers within the dimer in which the dimer interface is formed by the transmembrane β-strands 1, 2, and 19 (see Fig. 7*A, a*).

Second VDAC1 Oligomerization Sites—VDAC1 trimer, tetramer, hexamer, and higher oligomer (18–20, 38) formation require more than a single contact site between VDAC1 monomers. According to our computational study, VDAC1 cysteine residues Cys-127 and Cys-232 are found to be part of the second and the fourth VDAC1 unstable regions. We used BMOE, a thiol-specific cross-linker, for probing these cysteine residues. Indeed, dimers were obtained with VDAC1 containing a single cysteine (Cys-232 in β-strand 16), suggesting that the Cys-232 residues from each of two VDAC1 monomers face each other and are found in close proximity (<8 Å) within a dimer arrangement (see Fig. 4, *A* and *D, a*). Although according to recent VDAC1 topology models (14–16), Cys-232 faces the channel pore, our results suggest that this residue might also face the lipid phase and, in this position, be amenable for cross-linking. Furthermore, VDAC1 dimers also formed when a cysteine substitute was made at Ala-231 in β-strand 16 of ΔCys-rVDAC1(see Fig. 4*B*), supporting the proposal that β-strand 16 participates in a distinct contact site within the VDAC1 dimer (see Fig. 7*A, b*). These results are further supported by our computational study, which predicts that β-strand 17 participates

in protein-protein interaction. We identified Gln-249, a spatial neighbor of Ala-231 and Cys-232, to be very unstable and thus more likely to be involved in protein-protein interactions.

No dimers were obtained upon expression of a single cysteine residue, Cys-127, in β-strand 8 and subsequent exposure to BMOE (Fig. 4*A*), suggesting that Cys-127 in β-strand 8 is not found in the contact site responsible for the formation of dimeric VDAC1. This is surprising, because obtaining higher order oligomers in native VDAC1 upon cross-linking with BMOE (Fig. 4*A*) requires that both Cys-127 and Cys-232 be available for cross-linking. Moreover, Cys-127 is the most unstable of β-strands 7–9 (see Fig. 3*A*) and is likely to participate in protein-protein interactions. This may be explained by assuming that Cys-127 only becomes accessible for cross-linking once Cys-232 has already interacted with or has been cross-linked with BMOE. In other words, cross-linking of β-strand 16 by BMOE may induce conformational changes in the VDAC1 dimer that allow further cross-linking of β-strand 8 to form higher oligomeric forms (see model in Fig. 4*E*).

β-Strands 8 and 16 Play Role in Structuring VDAC1 Higher Ordered Oligomers—An association site centered at VDAC1 β-strand 8 was also predicted by our computational study. Residues Thr-116, Cys-127, and Gly-140 are unstable and likely to play an important role in this protein-protein interaction site. The results show that no dimers were obtained when BMOE was introduced into cells expressing VDAC1 containing only cysteine Cys-127, suggesting that β-strands 8 from each of two VDAC1 monomers are not facing each other. However, when both cysteine residues in the native rVDAC1 are available for cross-linking with BMOE, higher order oligomers (trimers, tetramers, hexamers, etc.) were formed (Fig. 4).

Our results also showed that mutations that are predicted to stabilize or destabilize the region of β-strands 8 and 16 affect
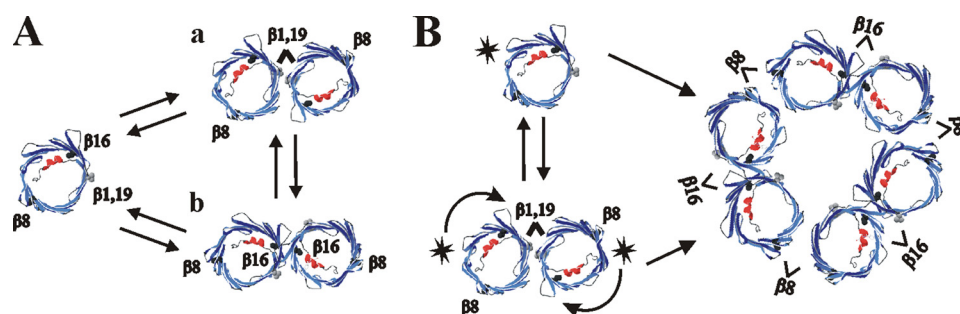
FIGURE 7. **A proposed model for apoptotic signal-induced VDAC1 oligomerization.** *A*, in the absence of an apoptotic signal, monomeric VDAC1 is present in a dynamic equilibrium with two forms of dimeric VDAC1: dimer interfaces involving unstable region I, comprising β-strands 1, 2, and 19 (*a*), or dimer interfaces composed from unstable region IV, comprising β-strands 16 and 17 (*b*). *B*, upon apoptosis induction, VDAC1 monomers or dimers undergo conformational changes (labeled with *asterisks*). Conformation-altered *VDAC1 dimers can interact with monomeric *VDAC1 to form trimers or with other dimers to form tetramers, hexamers, and higher oligomers.

VDAC oligomer formation. Expressing Q249L-VDAC1, which was predicted to stabilize the regions of β-strands 16 and 17, resulted in a decrease in VDAC oligomerization. On the other hand, expressing L125R, predicted to destabilize the region of β-strand 8, shifted VDAC1 to higher oligomeric forms. Stabilizing of β-strand 2 with the mutation S43L has no dramatic effect on VDAC1 oligomerization. Altogether, these results suggest that the two cysteine-containing β-strands 8 and 16 alone can allow formation of VDAC1 higher oligomers.

VDAC1 Oligomeric State and Conformational Changes Realized upon Apoptosis Induction—Recently, using chemical cross-linking and BRET2, we demonstrated that the oligomeric assembly of VDAC1 in cultured cells is highly enhanced upon induction of apoptosis by various inducers, all of which act via mitochondria but through different mechanisms (28, 29). These and other findings led us to propose that VDAC1 exists in a dynamic equilibrium between monomeric and oligomeric forms that shifts toward oligomerization upon apoptosis induction. We found that upon apoptosis induction, a new anti-VDAC1 antibody-reactive band corresponding to monomeric VDAC1 with modified electrophoretic mobility was obtained (Fig. 6*B*, *white arrow*). This suggests that apoptosis induced conformational changes in VDAC1 that were stabilized by EGS-mediated, intramolecular cross-linking. In addition, the dimer band obtained following apoptosis induction is wider than the dimer band obtained without apoptosis induction, suggesting that it is composed of heterogeneous dimers composed of a mixture of the two VDAC1 conformations (*i.e.* native and apoptosis-induced). In the higher oligomeric states, the bands look more homogenous, suggesting that they are composed of a single VDAC1 conformation, most likely the modified conformation (Fig. 6*B*).

Our results showed that cells incubated with the specific cross-linker, BMOE, which reacts with cysteine residues (native VDAC1 contains two cysteines), or EGS, which interacts with lysine residues (native VDAC1 contains 25 lysines), generated similar cross-linking products following apoptosis induction (Fig. 6*A*). Interestingly, an increase in the level of dimers and higher oligomers was obtained upon apoptosis induction and cross-linking with EGS, with identical levels of dimers and oligomers being formed with or without apoptosis induction and cross-linking with BMOE. This may reflect a situation whereby VDAC1 molecules are present in a dimeric arrangement and

can be cross-linked with BMOE but not with EGS (see Fig. 7*B*, *a*), implying that under physiological conditions, no lysine residues in the dimer are located in positions allowing for cross-linking with the 16.1-Å-long, inflexible EGS cross-linker.

Upon apoptosis induction, however, VDAC1 undergoes conformational changes that relocate lysine residues to positions that allow for their cross-linking by EGS. Such conformational changes upon apoptosis induction are reflected in the observed change in monomeric VDAC1 mobility (28) (Fig. 6*B*, *white arrow*).

Taking these findings together, we propose that under physiological conditions, a dynamic equilibrium exists between monomeric and dimeric forms of VDAC1, with strands β1, β2, β19 (Fig. 7*A*, *a*) or β16 and β17 (Fig. 7*A*, *b*) being found at the dimeric interface. Cross-linking of β-strands 16 by BMOE induces conformational change in a VDAC1 dimer that allows further cross-linking of β-strands 8 to form higher oligomers (Fig. 4, *A* and *D*). Upon apoptosis induction, formation of hexamers could occur through the same scenario, involving apoptosis-induced conformational changes (Fig. 6*B*). Such oligomerization begins with the equilibrium between monomeric and dimeric VDAC1 being shifted toward dimeric VDAC1, concomitant with conformational changes occurring to further encourage VDAC1 dimerization through interactions in the region of β strand 16. Next, the dimers interact with other VDAC1 monomers or dimers to form trimers, tetramers, hexamers, and larger oligomers, also probably via steps involving β-strand 8 (Fig. 7*B*).

In summary, we found that the interface between two VDAC1 monomers is formed by the unstable regions of the protein, β-strands 1, 2, and 19, and by a second contact site involving β-strands 16 and 17. We have shown that VDAC1 can exist under physiological conditions as a dimer that upon apoptosis induction can undergo conformational changes and further oligomerize to form higher oligomeric states involving β-strand 8. Further experimentation will delineate the exact nature of the conformational rearrangements of oligomeric VDAC1 in physiological and apoptosis conditions.

REFERENCES

1. Colombini, M. (2004) VDAC. The channel at the interface between mitochondria and the cytosol. *Mol. Cell Biochem.* **256**, 107–115
2. Shoshan-Barmatz, V., De Pinto, V., Zweckstetter, M., Raviv, Z., Keinan, N., and Arbel, N. (2010) VDAC. A multi-functional mitochondrial protein

regulating cell life and death. *Mol. Aspects Med.* **31,** 227–285

3. Shoshan-Barmatz, V., Israelson, A., Brdiczka, D., and Sheu, S. S. (2006) The voltage-dependent anion channel (VDAC). Function in intracellular signalling, cell life and cell death. *Curr. Pharm. Des.* **12,** 2249–2270

4. Lemasters, J. J., and Holmuhamedov, E. (2006) Voltage-dependent anion channel (VDAC) as mitochondrial governator. Thinking outside the box. *Biochim. Biophys. Acta* **1762,** 181–190

5. Saks, V., Guzun, R., Timohhina, N., Tepp, K., Varikmaa, M., Monge, C., Beraud, N., Kaambre, T., Kuznetsov, A., Kadaja, L., Eimre, M., and Seppet, E. (2010) Structure-function relationships in feedback regulation of energy fluxes *in vivo* in health and disease. Mitochondrial interactosome. *Biochim. Biophys. Acta* **1797,** 678–697

6. Granville, D. J., and Gottlieb, R. A. (2003) The mitochondrial voltage-dependent anion channel (VDAC) as a therapeutic target for initiating cell death. *Curr. Med. Chem.* **10,** 1527–1533

7. Shimizu, S., Ide, T., Yanagida, T., and Tsujimoto, Y. (2000) Electrophysiological study of a novel large pore formed by Bax and the voltage-dependent anion channel that is permeable to cytochrome *c. J. Biol. Chem.* **275,** 12321–12325

8. Tsujimoto, Y., and Shimizu, S. (2002) The voltage-dependent anion channel. An essential player in apoptosis. *Biochimie* **84,** 187–193

9. Thomas, L., Blachly-Dyson, E., Colombini, M., and Forte, M. (1993) Mapping of residues forming the voltage sensor of the voltage-dependent anion-selective channel. *Proc. Natl. Acad. Sci. U.S.A.* **90,** 5446–5449

10. Stanley, S., Dias, J. A., D'Arcangelis, D., and Mannella, C. A. (1995) Peptide-specific antibodies as probes of the topography of the voltage-gated channel in the mitochondrial outer membrane of *Neurospora crassa. J. Biol. Chem.* **270,** 16694–16700

11. De Pinto, V., Prezioso, G., Thinnes, F., Link, T. A., and Palmieri, F. (1991) Peptide-specific antibodies and proteases as probes of the transmembrane topology of the bovine heart mitochondrial porin. *Biochemistry* **30,** 10191–10200

12. Mannella, C. A., Colombini, M., and Frank, J. (1983) Structural and functional evidence for multiple channel complexes in the outer membrane of *Neurospora crassa* mitochondria. *Proc. Natl. Acad. Sci. U.S.A.* **80,** 2243–2247

13. Guo, X. W., Smith, P. R., Cognon, B., D'Arcangelis, D., Dolginova, E., and Mannella, C. A. (1995) Molecular design of the voltage-dependent, anion-selective channel in the mitochondrial outer membrane. *J. Struct. Biol.* **114,** 41–59

14. Bayrhuber, M., Meins, T., Habeck, M., Becker, S., Giller, K., Villinger, S., Vonrhein, C., Griesinger, C., Zweckstetter, M., and Zeth, K. (2008) Structure of the human voltage-dependent anion channel. *Proc. Natl. Acad. Sci. U.S.A.* **105,** 15370–15375

15. Hiller, S., Garces, R. G., Malia, T. J., Orekhov, V. Y., Colombini, M., and Wagner, G. (2008) Solution structure of the integral human membrane protein VDAC-1 in detergent micelles. *Science* **321,** 1206–1210

16. Ujwal, R., Cascio, D., Colletier, J. P., Faham, S., Zhang, J., Toro, L., Ping, P., and Abramson, J. (2008) The crystal structure of mouse VDAC1 at 2.3 Å resolution reveals mechanistic insights into metabolite gating. *Proc. Natl. Acad. Sci. U.S.A.* **105,** 17742–17747

17. Colombini, M. (2009) The published 3D structure of the VDAC channel. Native or not? *Trends Biochem. Sci.* **34,** 382–389

18. Zalk, R., Israelson, A., Garty, E. S., Azoulay-Zohar, H., and Shoshan-Barmatz, V. (2005) Oligomeric states of the voltage-dependent anion channel and cytochrome *c* release from mitochondria. *Biochem. J.* **386,** 73–83

19. Hoogenboom, B. W., Suda, K., Engel, A., and Fotiadis, D. (2007) The supramolecular assemblies of voltage-dependent anion channels in the native membrane. *J. Mol. Biol.* **370,** 246–255

20. Gonçalves, R. P., Buzhynskyy, N., Prima, V., Sturgis, J. N., and Scheuring, S. (2007) Supramolecular assembly of VDAC in native mitochondrial outer membranes. *J. Mol. Biol.* **369,** 413–418

21. Ujwal, R., Cascio, D., Chaptal, V., Ping, P., and Abramson, J. (2009) Crystal packing analysis of murine VDAC1 crystals in a lipidic environment reveals novel insights on oligomerization and orientation. *Channels* **3,** 167–170

22. Pedersen, P. L. (2008) Voltage dependent anion channels (VDACs). A brief introduction with a focus on the outer mitochondrial compartment's roles together with hexokinase-2 in the "Warburg effect" in cancer. *J. Bioenerg. Biomembr.* **40,** 123–126

23. Shoshan-Barmatz, V., Zakar, M., Rosenthal, K., and Abu-Hamad, S. (2009) Key regions of VDAC1 functioning in apoptosis induction and regulation by hexokinase. *Biochim. Biophys. Acta* **1787,** 421–430

24. Zaid, H., Abu-Hamad, S., Israelson, A., Nathan, I., and Shoshan-Barmatz, V. (2005) The voltage-dependent anion channel-1 modulates apoptotic cell death. *Cell Death Differ.* **12,** 751–760

25. Abu-Hamad, S., Arbel, N., Calo, D., Arzoine, L., Israelson, A., Keinan, N., Ben-Romano, R., Friedman, O., and Shoshan-Barmatz, V. (2009) The VDAC1 N-terminus is essential both for apoptosis and the protective effect of anti-apoptotic proteins. *J. Cell Sci.* **122,** 1906–1916

26. Gogvadze, V., Orrenius, S., and Zhivotovsky, B. (2006) Multiple pathways of cytochrome *c* release from mitochondria in apoptosis. *Biochim. Biophys. Acta* **1757,** 639–647

27. Abu-Hamad, S., Sivan, S., and Shoshan-Barmatz, V. (2006) The expression level of the voltage-dependent anion channel controls life and death of the cell. *Proc. Natl. Acad. Sci. U.S.A.* **103,** 5787–5792

28. Shoshan-Barmatz, V., Keinan, N., Abu-Hamad, S., Tyomkin, D., and Aram, L. (2010) Apoptosis is regulated by the VDAC1 N-terminal region and by VDAC oligomerization. Release of cytochrome *c*, AIF and Smac/Diablo. *Biochim. Biophys. Acta* **1797,** 1281–1291

29. Keinan, N., Tyomkin, D., and Shoshan-Barmatz, V. (2010) Oligomerization of the mitochondrial protein voltage-dependent anion channel is coupled to the induction of apoptosis. *Mol. Cell. Biol.* **30,** 5698–5709

30. Aram, L., Geula, S., Arbel, N., and Shoshan-Barmatz, V. (2010) VDAC1 cysteine residues. Topology and function in channel activity and apoptosis. *Biochem. J.* **427,** 445–454

31. Laemmli, U. K. (1970) Cleavage of structural proteins during the assembly of the head of bacteriophage T4. *Nature* **227,** 680–685

32. Naveed, H., Jackups, R., Jr., and Liang, J. (2009) Predicting weakly stable regions, oligomerization state, and protein-protein interfaces in transmembrane domains of outer membrane proteins. *Proc. Natl. Acad. Sci. U.S.A.* **106,** 12735–12740

33. Walther, D. M., Papic, D., Bos, M. P., Tommassen, J., and Rapaport, D. (2009) Signals in bacterial β-barrel proteins are functional in eukaryotic cells for targeting to and assembly in mitochondria. *Proc. Natl. Acad. Sci. U.S.A.* **106,** 2531–2536

34. Walther, D. M., Bos, M. P., Rapaport, D., and Tommassen, J. (2010) The mitochondrial porin, VDAC, has retained the ability to be assembled in the bacterial outer membrane. *Mol. Biol. Evol.* **27,** 887–895

35. Jimenez-Morales, D., and Liang, J. (2011) Pattern of amino acid substitutions in transmembrane domains of β-barrel membrane proteins for detecting remote homologs in bacteria and mitochondria. *PLoS One* **6,** e26400

36. Ferguson, A. D., Hofmann, E., Coulton, J. W., Diederichs, K., and Welte, W. (1998) Siderophore-mediated iron transport. Crystal structure of FhuA with bound lipopolysaccharide. *Science* **282,** 2215–2220

37. Adamian, L., Naveed, H., and Liang, J. (2011) Lipid-binding surfaces of membrane proteins. Evidence from evolutionary and structural analysis. *Biochim. Biophys. Acta* **1808,** 1092–1102

38. Malia, T. J., and Wagner, G. (2007) NMR structural investigation of the mitochondrial outer membrane protein VDAC and its interaction with antiapoptotic Bcl-xL. *Biochemistry* **46,** 514–525